Passive Double Pendulum in the Wake of a Cylinder Forced to Rotate Emulates a Cyclic Human Walking Gait

Adrian G. Carleton, Frank C. Sup IV, and Yahya Modarres-Sadeghi

Department of Mechanical and Industrial Engineering, University of Massachusetts, Amherst, MA 01003

E-mail: modarres@engin.umass.edu

Abstract. The goal of this work is to present a method based on fluid-structure interactions to enforce a desired trajectory on a passive double pendulum. In our experiments, the passive double pendulum represents human thigh and shank segments, and the interaction between the fluid and the structure comes from a hydrofoil attached to the double pendulum and interacting with the vortices that are shed from a cylinder placed upstream. When a cylinder is placed in flow, vortices are shed in the wake of the cylinder. When the cylinder is forced to rotate periodically, the frequency of the vortices that are shed in its wake can be controlled by controlling the frequency of cylinder's rotation. These vortices exert periodic forces on any structure placed in the wake of this cylinder. In our system, we place a double pendulum fitted with a hydrofoil at its distal end in the wake of a rotating cylinder. The vortices exert periodic forces on this hydrofoil which then forces the double pendulum to oscillate. We control the cylinder to rotate periodically, and measure the displacement of the double pendulum. By comparing the joint positions of the double pendulum with those of human hip, knee and ankle joint positions during walking, we show how the system is able to generate a human walking gait cycle on the double pendulum only using the interactions between the vortices and the hydrofoil.

1. Introduction

In this work, we investigate the possibility of obtaining trajectories similar to those of human walking gait in a passive double pendulum placed in fluid flow by using flow control strategies. We focus on the kinematics of the small-scale double pendulum that represents a human leg and we compare the trajectories obtained from this system with those from the human gait data.

Through physical interaction, the potential exists for a robot to assist a person during recovery from stroke, decline of motor functions due to age-related issues, or a disease. To accomplish this goal, research has focused on wearable robotic exoskeletons to create a symbiotic coupling between the user and the device with a goal to synchronize

the device with the user's motion for the device to feel natural [1]. However, current devices, such as Indego© [2], ReWalk© [3], and Esko Bionics© [4], suffer from being physically connected to the user causing interactions with the user's body that can create unwanted dynamics and discomfort at the interface. Another aspect of physical therapy is the use of body weight support mechanisms during sessions to allow a person to regain functionality without supporting one's full body weight [5]. Providing body weight support is done via harnesses (e.g., [6]), or more naturally and comfortably, using buoyancy as experienced when using an underwater treadmill. There is an example of a pneumatic exoskeleton suit that can be worn in the water, but this approach still physically connects to the user, impedes one's natural dynamics, and does not leverage unique dynamics of walking in the water [7]. In this paper, we present our work toward understanding how the dynamics of the fluid flow can be leveraged to assist or resist human limbs while walking underwater.

Previously, we had investigated the response of a minimally constrained hydrofoil (i.e., one hung from a string and otherwise free to move) placed in the wake of a cylinder [8]. In that work, we had considered the response of the hydrofoil when the cylinder was (i) fixed, (ii) forced to rotate in one direction, or (iii) forced to rotate periodically. This is an example of a Wake-Induced Vibrations problem, in which a body is placed downstream another and interacts with the wake of the upstream body (e.g., [9, 10, 11, 12]). Previous research had shown that if a cylinder placed in flow is forced to rotate in one direction [13, 14, 15, 16, 17, 18] or periodically in both directions [19, 20, 21, 22], its wake can be controlled. The shedding of vortices that are observed in the wake of a fixed cylinder placed in flow can be completely suppressed if the cylinder is forced to rotate in one direction with certain angular velocities or the shedding frequency can be altered if the cylinder is forced to rotate periodically within a range of angular velocities.

In our previous work [8], we investigated how a hydrofoil placed in the wake of such a cylinder reacts to the changes in the shedding patterns of the cylinder. We showed that when the cylinder is fixed, the hydrofoil interacts with the vortices that are shed in the cylinder's wake and oscillates at a frequency equal to the shedding frequency. This frequency increases with increasing flow velocity, following the Strouhal law, and cannot be controlled otherwise. When the cylinder is forced to rotate in one direction, the hydrofoil moves to the side of the wake and remains mainly static, as the rotation of the cylinder in one direction deflects the wake, which causes the hydrofoil to move to the side. When the cylinder is forced to rotate periodically, there is a range of rotation rates for which the shedding frequency equals the rotation frequency [23], and as a result the frequency at which the shed vortices interact with the hydrofoil can be controlled by controlling the rotation frequency. In this case, we found a range of frequencies for which the hydrofoil followed a figure-eight trajectory as it interacted with the shed vortices. This figure-eight trajectory included a relatively large displacement of the hydrofoil in the direction of the incoming flow (the inline direction). This inline oscillation is key to replicating a human gait, as the main component of motion while walking is parallel to

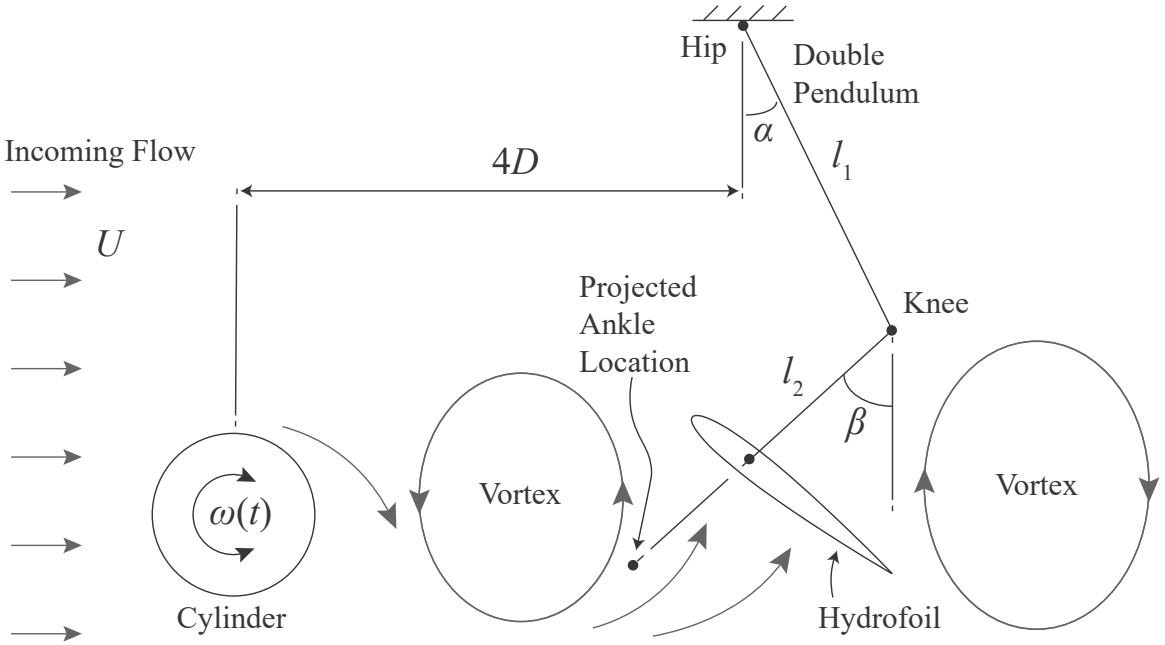

Figure 1. A schematic of the experimental setup together with an overview of the vortices that interact with the hydrofoil. The hydrofoil is attached to the tip of the lower limb, which represents the half-shank location. The dashed line represents the projection of the lower limb to the "ankle" location.

the flow.

Here, we show how the motion of this hydrofoil can force a double pendulum to follow trajectories similar to those of a human walking gait, when the hydrofoil is attached to a double pendulum. This work is part of a longer-term project to develop new methods of hydrotherapy for patients requiring assistance during gait training. In this project, a person walking on an underwater treadmill has hydrofoils affixed to their lower limbs and the fluid forces generated by the wake-hydrofoil interaction create assistive dynamics on their limbs to induce a desired gait pattern as required by the therapy. This system represents a novel approach to assisted gait training that allows for a non-contact interplay between the robot and human, where motive power and control commands are transmitted through the unconstrained fluid.

2. Experimental setup and method

The experiments were performed in a water tunnel with a test-section of 50 cm × 38 cm × 127 cm capable of flow velocities up to 1 m/s, with a uniform flow profile and a turbulence intensity of approximately 2% [24]. To replicate the kinematics of a human leg, a double pendulum, which is a common model of the limb, was designed and built, and a hydrofoil was mounted at the lower end of the pendulum (Figure 1). This pendulum was designed to minimize the friction in the joints, the mass, and the fluid forces acting upon it so the dynamics of the system would be dominated by the hydrofoil-

vortex interaction. Corrosion resistance was also a factor in material choices. To these ends, small ceramic ball bearings were selected and mounted in yokes 3D printed from PA2200 nylon using selective laser sintering (SLS). Thin aluminum rods were chosen as the link between joints. The top joint of the double pendulum was rigidly mounted to an extruded aluminum framework that was fixed to the test section of the water tunnel, and allowed for position adjustments in three directions. The hydrofoil was mounted rigidly at the lower end of the double pendulum. The upper limb of the double pendulum had a length of $l_1 = 12.9$ cm and the lower limb was $l_2 = 7.8$ cm. The length of the lower limb was selected such that when the hydrofoil was attached to its lower end, it would represent a hydrofoil that is attached approximately in the middle of the human's lower leg. The hydrofoil had a NACA 0012 profile with a chord length of $c = 75$ mm, and a span of $l = 100$ mm, and was mounted such that it projected from both sides of the bottom of the lower limb to minimize torques perpendicular to the axial direction, which could cause binding in the bearings. To replicate a human range of motion at each joint, each 3D printed yoke was designed with provisions for adding semi-compliant stops made from 0.022 in diameter spring wire. Joint rotation was limited to a range of $\alpha = -15^\circ$ to 45° at the hip and $\beta > 0^\circ$ at the knee. The hydrofoil was mounted at an angle of attack of approximately -8° relative to the lower link to keep the knee joint straight as it traveled upstream by keeping the joint under a small tension. The double pendulum was placed four diameters downstream the cylinder.

The upstream cylinder had a diameter of $D = 6$ cm, and spanned the width of the test section of the water tunnel. The cylinder was supported on a shaft which in turn was supported by corrosion-proof ball bearings mounted to streamlined vertical plates. These plates were extended above the surface of the water and connected to a rigid mounting frame made of extruded aluminum. One of these plates contained a shallow channel on the side against the test section's wall through which a thin toothed belt and pulley system was routed to connect the submerged cylinder to the drive motor. This motor was controlled with a National Instruments data acquisition card and a Simulink Real-Time model that allowed for precise control of the cylinder's velocity profile.

The experiments were filmed using a Phantom Miro M110 camera. The positions of the knee joint and the hydrofoil's 1/4 chord point were tracked using Adobe After Effects. Tracked data were then processed in MATLAB to determine the hip joint angle, α, and knee joint angle, β. These angles were calculated relative to the fixed hip joint location and a known true horizontal surface captured within the frame. Joint angles are reported as shown in Figure 1, with deflection in the upstream direction corresponding to a positive angle for the hip joint and a negative angle for the knee joint.

To visualize the flow, we used bubble image velocimetry (BIV) following the steps that we discussed in our previous work [8]. The major change in flow visualisation in the present work was that the 0.002-in-diameter platinum-iridium wire was taut upstream vertically (instead of horizontally) to enable a visualisation of the vortices from the side. PIVlab toolbox [25] in MATLAB was used to conduct the quantitative BIV analysis.

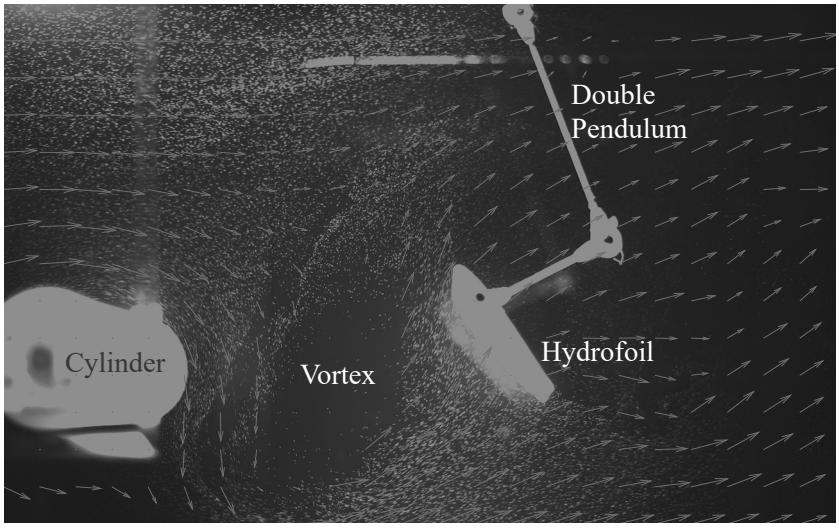

Figure 2. A snapshot from the actual experiment as the hydrofoil interacts with the vortex that is shed from the upstream cylinder. The arrows show the local velocity vectors calculated from the BIV results.

3. The experiments

In our previous work [8] we had shown that the frequency of the cylinder's rotation plays an important role in the observed response of the hydrofoil downstream, since the shedding frequency is controlled by the rotation frequency. We had shown that when the cylinder is forced to rotate periodically with a constant 1:1 ratio between CW and CCW rotations, then both figure-eight a nd l inear t rajectories a re observed in the hydrofoil's response. We had also observed that for lower values of cylinder's dimensionless frequency, inline oscillations are much larger in the hydrofoil's response. This inline component of the response is critical for us to be able to replicate the walking gait trajectory, since the walking gait trajectory for a human resembles a horizontal teardrop shape, with a large portion of the trajectory being in the walking direction. For our double-pendulum to emulate the walking gait, the walking direction will be in the direction of flow, and therefore we need to be able to induce a large inline motion. For these experiments, we considered several different combinations of system parameters. Here, we present the results of two sample cases only: case (i) at a reduced velocity of $U^* = U/f_nD = 2.4$ (where U is the incoming flow velocity and $f_n = 1.4$ Hz is the double pendulum first mode natural frequency in air), a dimensionless angular velocity of $\alpha = D\omega/2U = 2.3$ (where ω is the angular velocity of the cylinder), a dimensionless cylinder rotation frequency of $f^* = f_{cyl}D/U = 0.11$ (where f_{cyl} is the dimensional cylinder frequency in Hz), and a ratio of 2:3 for the CW to CCW rotation directions in each cycle of cylinder rotation, and case (ii) at $U^* = 2.7$, $\alpha = 2.1$, $f^* = 0.10$, and a CW to CCW ratio of 1:1. By looking at these two different cases, we will show that the results are not limited to a small sub-space in a relatively large parameter space of the system.

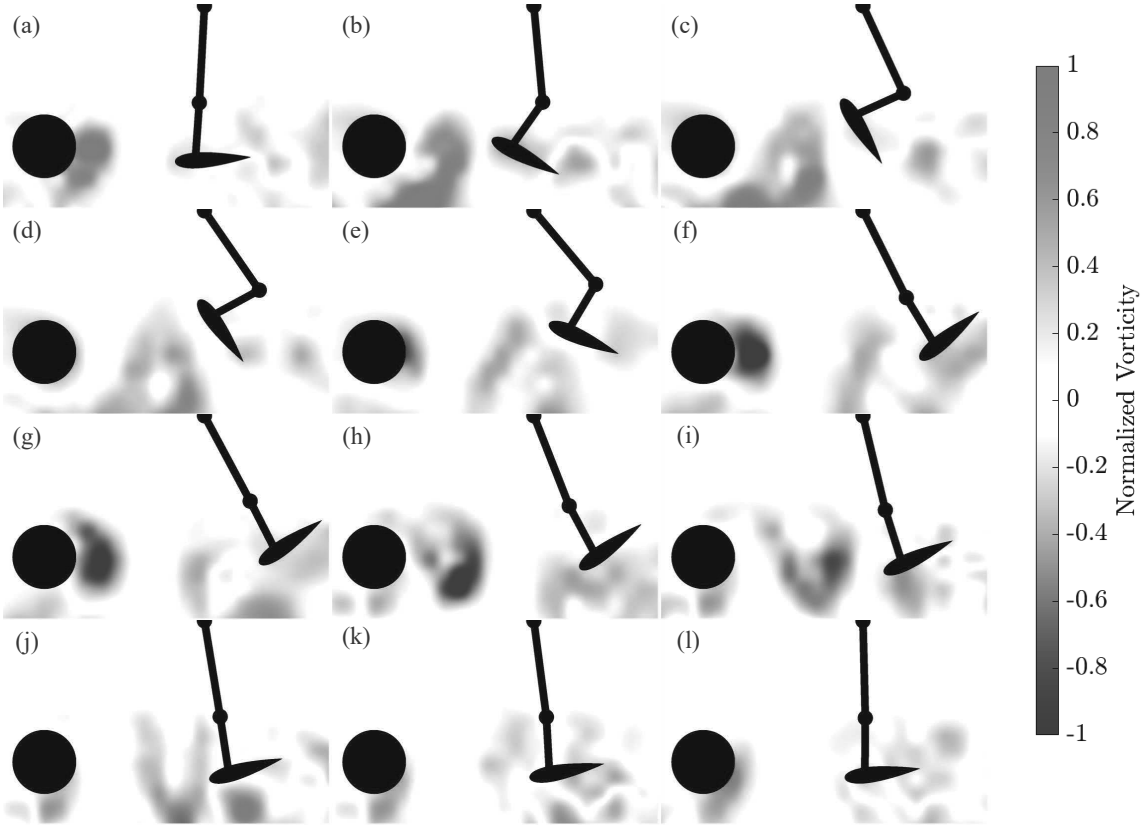

Figure 3. Snapshots of the interactions between the vortices shed in the wake of the cylinder and the hydrofoil over one gait cycle. The vorticity is normalized by the maximum value observed in the wake. The red (positive) vortex rotates in the CCW direction and the blue (negative) vortex rotates in the CW direction. See the supplementary material for an animation.

4. Hydrofoil-vortex interactions

To start, we consider case (i) and discuss how the vortices that are shed from the upstream cylinder interact with the hydrofoil. Figure 2 shows a snapshot of the actual experimental setup as the double pendulum and the hydrofoil attached to it interact with the incoming vortex. The arrows in the snapshot are the instantaneous velocity vectors of flow particles and provide an overall view of the flow behavior around the hydrofoil. In this snapshot, the vortex is forcing the hydrofoil to move to the right, which in turn causes the pendulum to "walk" in the direction of flow. Figure 3 shows twelve snapshots over one gait cycle of the double pendulum for this case. The first snapshot in the figure corresponds to when a positive vortex (rotating in the CCW direction) is shed from the lower side of the cylinder. In this snapshot, the double pendulum is straight and is moving upstream (i.e., toward the cylinder). In snapshot (b) the vortex that is traveling downstream starts interacting with the hydrofoil and forces the hydrofoil to go around the vortex. In this snapshot, the hydrofoil has started its upward motion. In snapshots (c) and (d), the positive vortex has already forced the hydrofoil to change its direction of motion dramatically and the hydrofoil is at a very large angle of attack with respect

to the incoming flow. In snapshot (e), the positive vortex is moved downstream, and the hydrofoil is rotating toward smaller angles of attack, and in snapshot (f), the vortex is clearly passed the hydrofoil and the pendulum is moving downstream (i.e., away from the cylinder). A negative vortex (rotating CW) is seen to be formed in snapshots (e) to (g). In snapshot (g), this vortex is fully developed and is in the wake. In snapshots (h) and (i), the negative vortex moves toward the hydrofoil, as the hydrofoil moves upstream. It is clear in snapshot (i) that when the hydrofoil sees the negative vortex, it is located such that the hydrofoil goes through the vortex, instead of around it, and slices the vortex into two pieces as seen in snapshots (j) and (k). In snapshot (k), the negative vortex is already divided into two counter rotating vortices highlighted by the blue and red colors in the top and below the hydrofoil. In snapshot (l), the double pendulum is at the same point in its cycle as in snapshot (a) and the cycle repeats. This scenario suggests that the oscillation frequency of the double pendulum is equal to the frequency of shedding of vortices from the upstream cylinder.

While two vortices are shed in the wake, only one of them (the positive vortex) exerts forces on the hydrofoil that cause changes in its motion. If both vortices that are shed in one cycle had similar interactions with the hydrofoil, then oscillations in the direction of flow would have been of a frequency twice the shedding frequency as observed before in the response of a flexibly-mounted cylinder placed in flow and allowed to oscillate in the direction of flow only [26]. However, here the two vortices interact with the hydrofoil differently. To clearly see the differences in the vortex-hydrofoil interactions for the positive and negative vortices, we should consider the relative location of the hydrofoil with respect to the incoming vortex when it approaches the vortex. In snapshot (b), the vortex is approaching the hydrofoil when the hydrofoil is already at a positive angle of attack and is moving toward the top of the vortex. This initial positioning then results in the hydrofoil traveling around the positive vortex. In snapshot (i), however, the hydrofoil approaches the vortex at a negative angle of attack and interacts with the side of the vortex first, which then results in the hydrofoil slicing the vortex into two counter rotating vortices. The fact that only one vortex causes dramatic change in the direction of the hydrofoil (and as a result the response of the double pendulum) suggests that a peak frequency should be observed in the response of the double pendulum at a frequency equal to the shedding frequency. We will discuss the trajectories of the double pendulum in the following section.

5. Sample gait trajectories of the double pendulum

Figure 4 shows sample snapshots of the pendulum motion over one cycle of oscillations for case (i) when the cylinder is forced to rotate with a ratio of 2:3 between the CW and CCW rotations. The dashed line that is extended from the hydrofoil downward projects the lower half of the lower leg and the black dot at the tip projects the location of the ankle. Human gait data are typically reported relative to the percent completion of each gait cycle in human kinematic studies, with gait cycles beginning and ending at

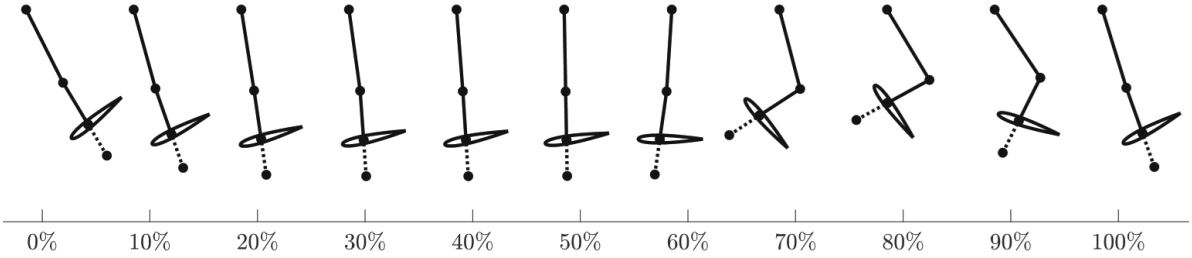

Figure 4. Snapshots of the pendulum motion over one gait cycle versus the percentage of a complete cycle for case (i), i.e., a CW to CCW ratio of 2:3 for the cylinder rotation.

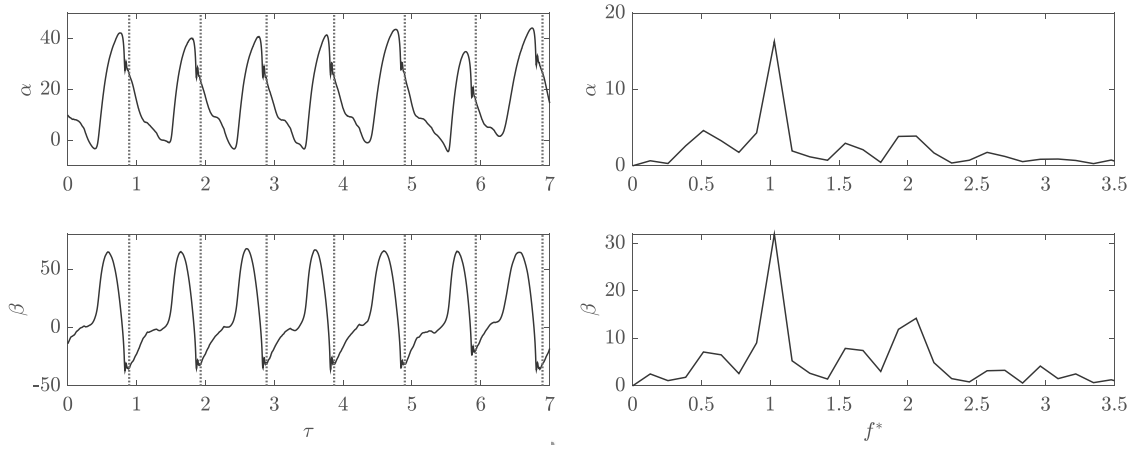

Figure 5. Time series and FFTs of the hip joint angle, α (upper row), and knee joint angle, β (lower row). In the plots, $\tau = tf_{cyl}$ and $f^* = f/f_{cyl}$ are dimensionless time and frequency, respectively. The vertical red lines in the time histories represent the end of each gait cycle.

the heel strike, when the foot first contacts the ground. Since in the double pendulum system of the present work there is no contact to demarcate each cycle, each gait cycle is defined as starting at 5% of a cycle after the point when the hydrofoil reaches its maximum upstream extension. This 5% offset accounts for the small amount of dwell time at this maximum forward position and the initial backward travel of the foot in the terminal swing phase of the gait before contacting the ground [27]. As we will see later in the text, this 5% also results in a close alignment of the peaks of the hip and knee angles between the double pendulum data and the human gait data.

Sample time histories for the hip joint angle, α, and the knee joint angle, β, together with their corresponding frequency contents are given in Figure 5 for case (i). The time histories show repeatable gait cycles for both angles over several cycles. The FFT plots corresponding to both time histories exhibit a main peak at a dimensionless frequency of $f^* = f/f_{cyl} = 1$, which means that oscillations of both joints are synchronized with the forcing frequency, which is also equal to the shedding frequency. This is the result of the fact that only one of the two vortices that are shed in the wake causes a change

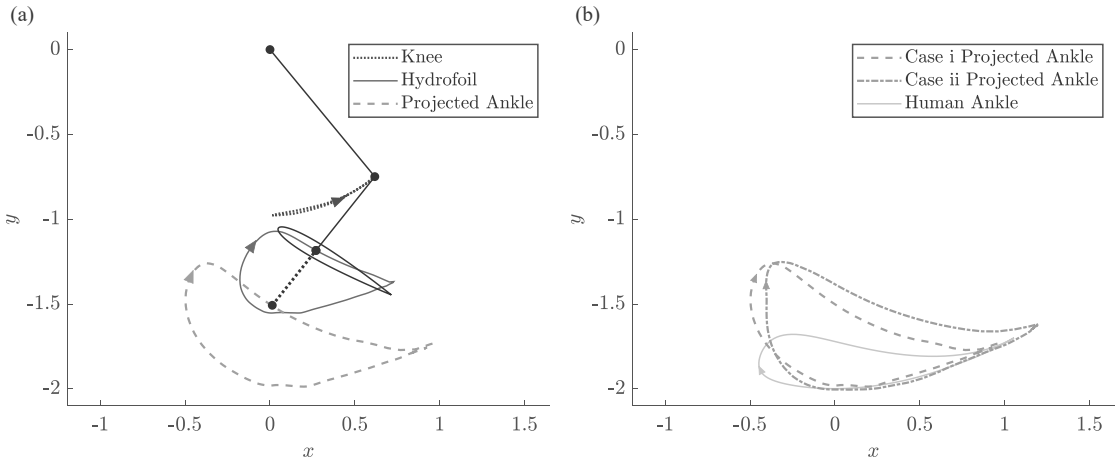

Figure 6. (a) Trajectories of the knee, the location of the hydrofoil, and the projected location of the ankle over a gait cycle shown as the averaged values of several gait cycles. (b) Ankle trajectories from the sample cases of the double-pendulum results plotted on top of the average results from human walking gait. The axes are normalized by l_1.

in the direction of motion of the hydrofoil, as we saw in the flow visualisation results of Section 4. The existence of the second vortex and its interaction with the hydrofoil are reflected in the FFT plots of Figure 5 as small peaks at the second harmonic. The interaction with the second vortex does not change the direction of hydrofoil's motion, but it is significant enough to be observed in the FFT plots.

The plot of Figure 6(a) highlights the trajectories observed at the knee, half-shank (the location of the hydrofoil), and the ankle. The horizontal teardrop like trajectories that are observed at the hydrofoil and ankle locations resemble those observed in actual human gaits, with a 1:1 frequency ratio between the x and y components of the response. This comparison is made in Figure 6(b) where the ankle trajectories from the two sample cases discussed here are plotted on top of the average human gait trajectory based on the data provided in the literature [27]. It is observed in the plot of Figure 6(b) that the trajectories cover a very similar distance in the x-direction, but in the y-direction, the double pendulum trajectories are larger. While quantitative differences are observed, the trajectories from the double pendulum follow a pattern very similar to the human gait trajectories. One should also consider that the two pendulum trajectories are two sample cases in a relatively large parameter space. A more comprehensive comparison between the double pendulum results and the human gait data is provided in the following section.

6. Double pendulum response in comparison with human walking gait

An overall view of how the hip joint angle, α, and the knee joint angle, β, vary in each gait cycle of the double pendulum is given in Figure 7 for the two sample cases discussed here. The plots on the left column correspond to case (i) and the plots on the right

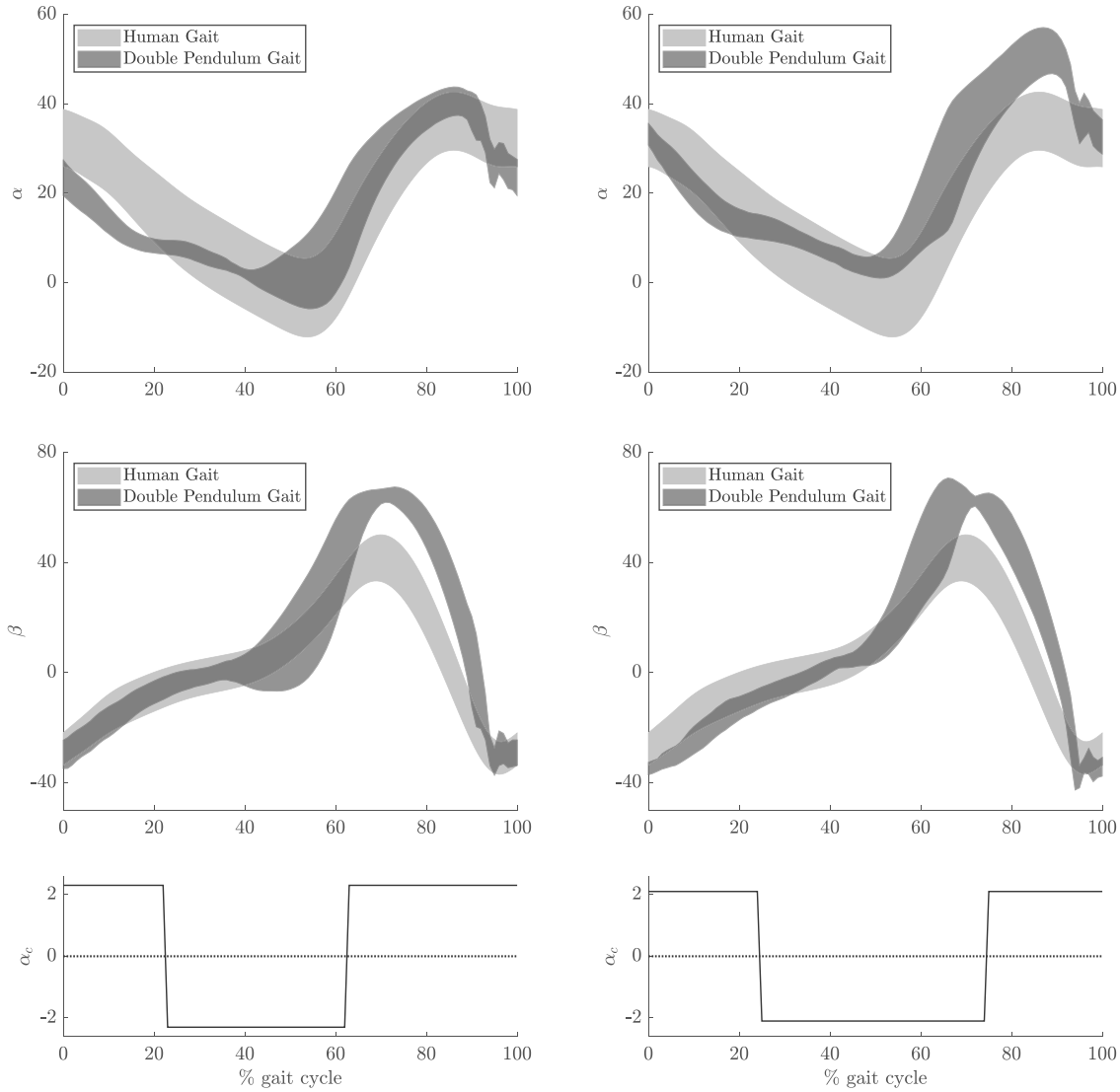

Figure 7. Average responses of the hip joint angle, α (first row), and knee joint angle, β (second row), based on the double pendulum response and normal human walking gaits, together with the input normalized angular velocity, α_c, given to the upstream cylinder, for case (i) a 2:3 ratio between the CW and CCW rotations and $U^* = 2.1$ (left), and case (ii), a 1:1 ratio between the CW and CCW rotations and $U^* = 2.3$. (right).

column to case (ii). The waveforms of the input dimensionless angular velocities are also given in the figure for both cases. In the plots, the gait response of the double pendulum are compared with those of human gait. The human data are obtained from a publicly available data set of lower limb kinematics [27]. This data set contains joint angles for ten test subjects walking at a range of speeds, and the data used here are for 0.8 m/s. In the plots of Figure 7, we show the range for these data as well as the data from our double-pendulum results that is found as the mean of the data plus minus one standard deviation.

The results from the two sample cases of the double pendulum response shown in

the figure follow a similar pattern, despite the fact that the input signal that forced the cylinder rotation and the reduced velocity were different in these cases. Also, the double pendulum results follow a trend similar to what is observed in human walking gait. The hip angle of the double pendulum decreases initially to reach a local minimum at approximately 55% of the gait cycle. The hip angle then increases until it reaches a local maximum at approximately 85% of the gait cycle. The knee angle increases initially in the first 15% of the gait cycle, and then the rate of its increase decreases, followed by another high-rate increase starting around 45% of the gait cycle, leading to a local maximum at approximately 70% of the gait cycle. This angle then decreases monotonically until the end of the cycle. One important feature in the data is that the local minimum of the hip angle (at approximately 55%) and the local maximum of the knee angle (at approximately 70%) occur at comparable points in the gait cycle for the double pendulum and the human gait data. It is also important to note that the local minimum of the hip angle and the local maximum of the knee angle occur at two different points during the cycle, which implies that the hysteresis loop (the horizontal teardrop trajectory) is observed in the trajectory of the double-pendulum ankle as we saw earlier in the plots of Figure 6.

These similarities between the double-pendulum gait cycles and the human gait cycles are obtained despite several differences between the two systems. Most notable is the fact that the double pendulum is a passive system versus a human limb with musculoskeletal system with active and passive dynamics. Another difference lies in the fact that the double pendulum system does not have any contact with the ground, and therefore the ground forces that act on a human leg during a cycle are missing in the double pendulum gait. In the human gait cycle, due to the ground impact, there is a small amount of overshoot in the hip joint before the beginning of the next gait cycle. This overshoot is not present in the double-pendulum case, which uses a 5% offset from the maximum upstream position as the start of the gait cycle. Lastly, the hip joint location is not fixed in the human walking data, and it oscillates, while in the double pendulum setup, the upper hinge is fixed. The human gait pelvis angle oscillates around a mean value of approximately 10° [27], and is another source for differences observed between the double-pendulum results and the human walking gait.

7. Discussion and Conclusions

We have presented a design to emulate the human walking gait using a passive double pendulum placed in flow. The double pendulum's motion is induced by forcing a cylinder placed upstream the double pendulum to rotate at a desired frequency and follow a desired waveform, thereby controlling the frequency and strength of the vortices that are shed in its wake. These vortices in turn interact with a hydrofoil that is attached to the tip of the lower limb of the double pendulum and force it to follow a desired path.

Through a detailed BIV analysis, we show that of the two vortices that are shed in the wake of the upstream cylinder, one interacts with a hydrofoil such that it forces

the hydrofoil to go around the vortex. The second vortex, however, is sliced to two smaller vortices by the hydrofoil during the upstream motion of the double pendulum and does not influence the hydrofoil's motion significantly. The result of this interaction is a trajectory with a horizontal teardrop shape at the ankle location of the double pendulum that resembles the trajectory measured in the human gait cycle. When we compare the hip angle and the knee angle measured in the double pendulum response with those from the human gait cycle, we observe very important similarities: In both the human gait and the double pendulum responses the peaks of the hip angle and the knee angle occur at two different points in the gait cycle, which result in a hysteresis loop (or the horizontal teardrop shape trajectory), as opposed to a trajectory that would have traversed the same path moving forward and backward. The relative locations of these two peaks in the hip angle and the knee angle time histories are also comparable for both cases.

We have discussed two sample cases for the double pendulum results for two sets of parameters. The parameter space for this system is a very large one in which one can adjust different parameters to obtain a desired motion. These parameters include the relative length of the two limbs of the double pendulum, the frequency at which the upstream cylinder is forced to rotate, the wavefrom with which the cylinder is forced, the distance between the upstream cylinder and the double pendulum, the exact location where the hydrofoil is attached to the double pendulum, and the value of the reduced velocity, to name a few. A comprehensive parametric study that would consider all these parameters was not the goal of this work. The goal was to show that it is possible to obtain human-gait like response in a passive double pendulum through the manipulation of the incoming flow upstream, and without directly interacting with the double pendulum otherwise. We have shown that this is possible for some combinations of the parameters in the large parameter space of this system. The results of this work demonstrate the feasibility of this approach on a larger-scale, immersive robotic system. The system would manipulate the incoming flow to induce forces on hydrofoils attached to a person's limbs which would guide them into a prescribed gait trajectory while walking on an underwater treadmill.

Acknowledgment

This work is supported by the National Science Foundation through grant number CMMI 2024409.

References

[1] A. Rodríguez-Fernández, J. Lobo-Prat, and J. M. Font-Llagunes, "Systematic review on wearable lower-limb exoskeletons for gait training in neuromuscular impairments," *Journal of neuroengineering and rehabilitation*, vol. 18, no. 1, pp. 1–21, 2021.

[2] C. Tefertiller, K. Hays, J. Jones, A. Jayaraman, C. Hartigan, T. Bushnik, and G. F. Forrest,

"Initial outcomes from a multicenter study utilizing the indego powered exoskeleton in spinal cord injury," *Topics in spinal cord injury rehabilitation*, vol. 24, no. 1, pp. 78–85, 2018.

[3] A. Esquenazi, M. Talaty, A. Packel, and M. Saulino, "The rewalk powered exoskeleton to restore ambulatory function to individuals with thoracic-level motor-complete spinal cord injury," *American journal of physical medicine & rehabilitation*, vol. 91, no. 11, pp. 911–921, 2012.

[4] C. Bach Baunsgaard, U. Vig Nissen, A. Katrin Brust, A. Frotzler, C. Ribeill, Y.-B. Kalke, N. León, B. Gómez, K. Samuelsson, W. Antepohl *et al.*, "Gait training after spinal cord injury: safety, feasibility and gait function following 8 weeks of training with the exoskeletons from ekso bionics," *Spinal cord*, vol. 56, no. 2, pp. 106–116, 2018.

[5] A. Wernig and S. Müller, "Laufband locomotion with body weight support improved walking in persons with severe spinal cord injuries," *Spinal Cord*, vol. 30, no. 4, pp. 229–238, 1992.

[6] J. Hidler, D. Brennan, D. Nichols, K. Brady, T. Nef *et al.*, "Zerog: overground gait and balance training system." *Journal of Rehabilitation Research & Development*, vol. 48, no. 4, 2011.

[7] T. Miyazaki, H. Suzuki, D. Morisaki, T. Kanno, R. Miyazaki, T. Kawase, Y. Kawakami, and K. Kawashima, "Underwater walking using soft sensorless gait assistive suit," in *2019 IEEE/SICE International Symposium on System Integration (SII)*. IEEE, 2019, pp. 237–242.

[8] T. M. Currier, A. G. Carleton, and Y. Modarres-Sadeghi, "Dynamics of a hydrofoil free to oscillate in the wake of a fixed, constantly rotating or periodically rotating cylinder," *Journal of Fluid Mechanics*, vol. 923, p. A21, 2021.

[9] G. R. S. Assi, P. W. Bearman, and J. R. Meneghini, "On the wake-induced vibration of tandem circular cylinders: the vortex interaction excitation mechanism," *Journal of Fluid Mechanics*, vol. 661, p. 365–401, 2010.

[10] P. Bearman, "Circular cylinder wakes and vortex-induced vibrations," *Journal of Fluids and Structures*, vol. 27, no. 5-6, pp. 648–658, 2011.

[11] G. R. d. S. Assi, P. Bearman, B. S. Carmo, J. R. Meneghini, S. J. Sherwin, and R. Willden, "The role of wake stiffness on the wake-induced vibration of the downstream cylinder of a tandem pair," *Journal of Fluid Mechanics*, vol. 718, pp. 210–245, 2013.

[12] F. Huera-Huarte and M. Gharib, "Vortex-and wake-induced vibrations of a tandem arrangement of two flexible circular cylinders with far wake interference," *Journal of Fluids and Structures*, vol. 27, no. 5-6, pp. 824–828, 2011.

[13] H. Badr, M. Coutanceau, S. Dennis, and C. Menard, "Unsteady flow past a rotating circular cylinder at reynolds numbers 10^3 and 10^4," *Journal of Fluid Mechanics*, vol. 220, pp. 459–484, 1990.

[14] F. Diaz, J. Gavaldà, J. Kawall, J. Keffer, and F. Giralt, "Vortex shedding from a spinning cylinder," *The Physics of fluids*, vol. 26, no. 12, pp. 3454–3460, 1983.

[15] S. Kumar, C. Cantu, and B. Gonzalez, "Flow past a rotating cylinder at low and high rotation rates," *Journal of Fluids Engineering*, vol. 133, no. 4, 2011.

[16] S. Mittal and B. Kumar, "Flow past a rotating cylinder," *Journal of fluid mechanics*, vol. 476, pp. 303–334, 2003.

[17] A. Rao, A. Radi, J. Leontini, M. Thompson, J. Sheridan, and K. Hourigan, "A review of rotating cylinder wake transitions," *Journal of Fluids and Structures*, vol. 53, pp. 2 – 14, 2015, special Issue on Unsteady Separation in Fluid-Structure Interaction–II. [Online]. Available: http://www.sciencedirect.com/science/article/pii/S0889974614000668

[18] B. Seyed-Aghazadeh and Y. Modarres-Sadeghi, "An experimental investigation of vortex-induced vibration of a rotating circular cylinder in the crossflow direction," *Physics of Fluids*, vol. 27, no. 6, p. 067101, 2015.

[19] P. Tokumaru and P. Dimotakis, "Rotary oscillation control of a cylinder wake," *Journal of Fluid Mechanics*, vol. 224, pp. 77–90, 1991.

[20] ——, "The lift of a cylinder executing rotary motions in a uniform flow," *Journal of Fluid Mechanics*, vol. 255, pp. 1–10, 1993.

[21] N. Fujisawa, K. Ikemoto, and K. Nagaya, "Vortex shedding resonance from a rotationally oscillating

cylinder," *Journal of Fluids and Structures*, vol. 12, no. 8, pp. 1041–1053, 1998.

[22] M.-H. Chou, "Synchronization of vortex shedding from a cylinder under rotary oscillation," *Computers & fluids*, vol. 26, no. 8, pp. 755–774, 1997.

[23] L. Du and C. Dalton, "Les calculation for uniform flow past a rotationally oscillating cylinder," *Journal of Fluids and Structures*, vol. 42, pp. 40–54, 2013.

[24] B. Seyed-Aghazadeh, D. W. Carlson, and Y. Modarres-Sadeghi, "Vortex-induced vibration and galloping of prisms with triangular cross-sections," *Journal of Fluid Mechanics*, vol. 817, pp. 590–618, 2017.

[25] W. Thielicke and R. Sonntag, "Particle image velocimetry for MATLAB: Accuracy and enhanced algorithms in PIVlab," *Journal of Open Research Software*, vol. 9, 2021. [Online]. Available: https://doi.org/10.5334/jors.334

[26] T. D. Gurian, T. Currier, and Y. Modarres-Sadeghi, "Flow force measurements and the wake transition in purely inline vortex-induced vibration of a circular cylinder," *Physical Review Fluids*, vol. 4, no. 3, p. 034701, 2019.

[27] E. Reznick, K. Embry, R. Neuman, E. Bolivar, N. Fey, and R. Gregg, "Lower-limb kinematics and kinetics during continuously varying human locomotion," Oct 2021. [Online]. Available: https://springernature.figshare.com/collections/Lower-limb_Kinematics_and_Kinetics_During_Continuously_Varying_Human_Locomotion/5175254/1